BACHELORARBEIT / BACHELOR'S THESIS

Titel der Bachelorarbeit / Title of the Bachelor's Thesis

„Solar Rotation“

verfasst von / submitted by

Dominic Förster

angestrebter akademischer Grad / in partial fulfilment of the requirements for the degree of

Bachelor of Science (BSc)

Wien, 2023/24 / Vienna, 2023/24

Studienkennzahl lt. Studienblatt / degree programme code as it appears on the student record sheet:	UA 033661
Studienrichtung lt. Studienblatt / degree programme as it appears on the student record sheet:	Bachelorstudium Astronomy
Betreut von / Supervisor:	Univ.-Prof. Dr. Arnold Hanslmeier

Abstract

This thesis explores the relationship between solar differential rotation, the underlying theoretical concepts of the dynamo theory, and the resulting solar activity phenomena. Further observation of these effects can lead to an improvement of our solar models, which can help to gain a deeper understanding of the dynamics in the Sun and other stars. Specifically for the Earth, which is often influenced by solar events, it can be helpful to make space weather forecasts to reduce the negative effects of these events. The work is structured into three different parts.

The first part provides a historical overview of the methods used to observe the solar differential rotation, beginning from Galileo's pioneer work in 1630 with the discovery of sunspots through spectroscopic observation to the current helioseismic techniques. This review provides detailed insight into the solar rotation profile and large-scale motions.

In the second part, this knowledge of differential rotation is used in the solar dynamo theory, where the famous Ω-effect illustrates the link between differential rotation and magnetic field dynamics. This part explores the two main principles: $\Omega\alpha$-model by Parker and the Babcock-Leighton (BL) to explain the general magnetic field dynamics.

The last part contains an empirical study that demonstrates the differential rotation of sunspots. Images from the Helioseismic Magnetic Imager (HMI) onboard the Solar Dynamics Observatory (SDO) were utilized. The necessary measurements and calculations were performed with several Python packages.

Contents

Abstract **i**

1. Introduction **1**
1.1. Motivation . . . 1
1.2. Goal of This Thesis . . . 1

2. Theory of Stellar Structure **3**
2.1. Origin of Stellar Rotation . . . 3
2.2. Stefan-Boltzmann Law . . . 3
2.3. Doppler Effect . . . 4
2.4. Zeeman Effect . . . 4

3. Solar Interior and Atmosphere **5**
3.1. Core . . . 6
3.2. Radiative Zone . . . 6
3.3. Convective Zone . . . 6
3.4. Photosphere . . . 6
3.5. Chromosphere . . . 7
3.6. Corona . . . 7

4. Solar Activity **9**
4.1. Sunspots . . . 9
4.2. 10.7cm Solar Flux ($F_{10.7}$) . . . 11
4.3. Solar Wind . . . 11
4.4. Solar Flares (SFs) and Coronal Mass Ejections (CMEs) . . . 11
4.5. Coronal Holes (CHs) . . . 12
4.6. Prominences and Filaments . . . 12
4.7. Plages Regions . . . 12

5. Solar Rotation Observation **13**
5.1. History . . . 13
5.1.1. Tracer Motion . . . 13
5.1.2. Spectroscopy . . . 14
5.1.3. Helioseismology . . . 14
5.1.4. Comparison . . . 14
5.2. Current State . . . 15
5.2.1. Differential Rotation . . . 15

5.2.2. Meridional Flow 16

6. Dynamo Theory **19**
6.1. Observational Effects 19
6.2. Theory 19
6.2.1. Ω-Effect 20
6.2.2. α-Effect 21
6.2.3. Babcock–Leighton Model 21

7. Sunspots as Tracers **23**
7.1. Method 23
7.1.1. Image Processing 23
7.1.2. Calculation of the Rotation Rate 25
7.2. Result 26
7.3. Discussion 27

8. Conclusion **29**

Bibliography **31**

Appendix A. Download FITS Code **35**

Appendix B. Sunspots Tacking Code **37**

Appendix C. Calculation of the Rotation Rate Code **45**

Appendix D. Directory Structure **51**

1. Introduction

1.1. Motivation

The rotation of the Sun is an interesting topic in solar astrophysics because it is differential, contrasting with the rigid body rotation of our Earth. This differential rotation is directly connected to the magnetic dynamics within the Sun, the resulting solar activity, and the majority of space weather effects. Furthermore, studies of differential rotation can help improve solar models, especially the dynamo theory. An improved model could help predict upcoming solar events and reduce their negative influence on Earth. Additionally, the Sun can also be seen as a laboratory for understanding stellar evolution as a whole.

1.2. Goal of This Thesis

My scope for this work is to provide a comprehensive overview of solar rotation and its associated effects, including both observable phenomena and theoretical aspects. To achieve this, I begin by introducing key physical concepts often used in solar astrophysics, followed by an exploration of the solar interior and atmosphere, along with various phenomena related to solar activity. After this explanation, I will examine the various methods that have been used to observe the solar differential rotation, concluding with the current understanding and theories about the rotation profile. This foundation will be used to build the connection to today's known dynamo theories and the resulting solar activity. Finally, I will do my own empirical analysis of sunspots to show their differential rotation behavior.

2. Theory of Stellar Structure

2.1. Origin of Stellar Rotation

Star formation occurs in cold and dense gas clouds within the intergalactic medium. A protostar forms when such a cloud collapses under its own gravitational force. Due to the angular momentum conservation, the protostar starts to rotate, meaning that stellar rotation originates early in the star formation process. It is also possible that the cloud already has an initial rotation rate; in this case, the rotation rate will increase with the collapse. During the early stages, the stellar rotation can be influenced by accretion from the protostellar disk, the pirouette effect, and the jets of the protostellar disk. The accretion of particles from the disk and the pirouette effect can accelerate the protostar's rotation rate. Moreover, the centrifugal force on the protostar increases, to prevent the protostar's explosion, stellar phenomena like jets are believed to decrease the angular momentum. This allows the protostar to reach an equilibrium state between gravitational and centrifugal force. As the star evolves, its rotation rate can change due to mass ejections combined with magnetic fields, which transport angular momentum away from the star and decreasing the rotation rate once again. Additionally, the pressure force generated by atomic fusion inside the star contributes to its stability. It has also been observed that stars with higher rotation rates decrease their rotation rate more rapidly because the rotation rate is linked to stellar activity, which can lead to larger mass ejections. (Kutner, 2003)

2.2. Stefan-Boltzmann Law

The Stefan-Boltzmann law is an idealized model to represent the radiation of a body as black body radiation. It is proportional to the fourth power of the temperature T^4; in astrophysics, the concept of a black body is often used to describe the total luminosity L of a star. To derive the luminosity from the Stefan-Boltzmann law only the multiplication with the surface area of the star $4\pi R^2$ is needed, which leads to the relation shown in Equation (2.1).

$$L \propto R^2 T^4 \tag{2.1}$$

This relation can explain why some solar activity features appear darker or brighter due to a temperature difference. (Kutner, 2003)

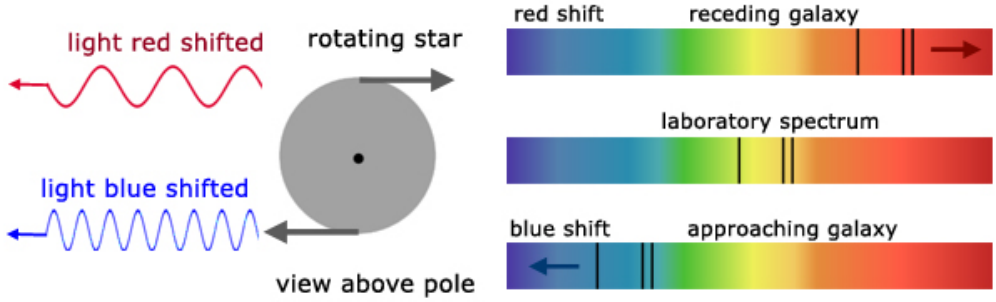

Figure 2.1.: The figure illustrates the impact on spectral lines when the object is rotating. A red shift is observed on one limb, while a blue shift is visible on the opposite limb. (from a-levelphysicstutor.com)

2.3. Doppler Effect

The Doppler effect is widely used in physics and astrophysics to determine the proper motions of objects. The main concept is to make a spectroscopic observation of the object and measure the Doppler shift $\Delta\lambda$ between the observed spectral line position and its rest wavelength λ_0. This offset can either be positive, leading to a stretched wave, known as a redshift, indicating the object is moving away from the observer, or it is negative, resulting in a squeezed wave, referred to as a blueshift, indicating the object is moving towards the observer. Both cases are illustrated in Figure 2.1. Using the simple Equation (2.2), the radial velocity of the object can be calculated, where c represents the speed of light in vacuum. If the line of sight is directly aligned with the rotation axis, no shift in the spectrum is measurable. For spectroscopic observation on Earth, it is crucial to account for the fact that the Earth's atmosphere produces spectral lines in the spectrum too. The spectrum of the observed object and the Earth's atmosphere are overlapping.

$$v_r = c \cdot \frac{\Delta\lambda}{\lambda_0}, \text{ if } v_r \ll c \tag{2.2}$$

2.4. Zeeman Effect

The Zeeman effect is a quantum mechanical effect in spectroscopic observations when a magnet field interacts with an observed object's electrons. If the field is applied, the energy level of the electrons constantly changes, leading to a splitting of the spectral lines. (Kutner, 2003)

3. Solar Interior and Atmosphere

The interior and atmosphere of the Sun can be divided into different parts. When an observation in the visible light range is done, a thin layer in the solar atmosphere, called the photosphere, is typically seen, commonly referred to as the solar surface. Underneath the photosphere are the inner layers of the Sun, containing the convective zone, radiative zone, and core. The chromosphere and the corona are above the photosphere, also called the outer layers or atmosphere. Figure 3.1 illustrates the different layers and approximated thicknesses. Each layer, starting from the core outwards, will be briefly described in the following sections.

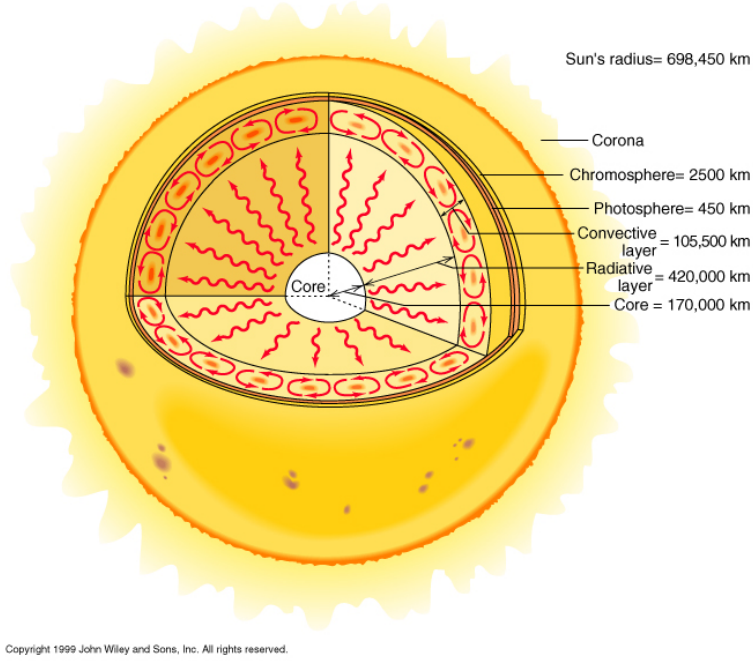

Figure 3.1.: The illustration shows the anatomy of the Sun, highlighting its primary energy transport mechanisms: radiation and convection. The photosphere is identified with the solar surface, as the layers of the outer atmosphere are optically thin. The solar radius is measured from the center to the outer edge of the photosphere. (from ESO)

3.1. Core

The primary energy source of the Sun is atomic fusion that takes place in the core. The Sun is categorized as a G2 main sequence star and primarily produces helium from hydrogen through the proton-proton (pp) chain reaction. The thermal fusion in the core is possible because of the extreme temperature of around 15 million K. Solar neutrinos, generated during the pp-chain reaction, interact minimally with matter on their journey from the core to the Earth's surface, attributed to their significant mean free path length. This characteristic allowed Bahcall and Davis (1976) to use such neutrinos to confirm nuclear fusion processes within the solar core, providing direct evidence of the process.

3.2. Radiative Zone

During the pp-reaction, photons are emitted which, due to their constant interaction with other particles in the core, take thousands of years to reach the radiative zone. The name of the zone is derived from the predominant mechanism of energy transport in this region. In the radiative zone, temperatures are lower than in the core, ranging from around 7 million Kelvin at the bottom to 2 million K at the top. At these temperatures, intact atoms can exist, that absorb and re-emit the photons at slightly longer wavelengths, a process characteristic of radiative transfer. The photons undergo a so-called *random walk motion*, constantly changing their wavelength from gamma rays to visible light through these repeated interactions. (Kutner, 2003)

3.3. Convective Zone

After the radiative zone, the photons reach the convective zone, whose name also derives from the predominant energy transport mechanism. In this layer, the photons heat the gas, raising its temperature. However, the gas is not hot enough to re-radiate all the energy efficiently, so the energy is transported upward with the gas itself. This process is analogous to heating water: as the water at the bottom of a pot heats up, it rises to the surface in bubbles, cools down, and then sinks again. Similarly, in the convective zone, heated gas containing the energy rises to the surface, expands, cools, and descends. This convective motion effectively transports energy from the solar interior to the outer layers. (Kutner, 2003)

3.4. Photosphere

The photosphere is the layer associated with the surface of the Sun because a continuous emission spectrum can be observed. The primary reason for this continuous spectrum is the presence of H^- ions. These ions require only a small amount of energy to detach their additional electron and emit it with a specific kinetic energy. Photons absorbed by the ions supply this energy, enabling nearly every photon to trigger this process. Due to

the varying energies of the incoming photons, electrons are emitted with different kinetic energies. Consequently, the reverse process generates the continuous emission spectrum that is observable. The peak in this spectrum corresponds to a black body temperature of around 5500 K, reflecting the effective solar surface temperature.

As the distance from the center increases, the density of the solar gas decreases without a sharp edge, unlike what is typical for the Earth, making it challenging to define a sharp surface boundary. This density gradient also leads to another effect on the photosphere, known as *limb darkening*. The limb appears darker due to the lower density. This phenomenon can be explained by the optical depth τ concept, which is proportional to the density. Along any line of sight, the visibility extends until $\tau \leq 1$. At the limb, the line of sight passes through less dense gas, whereas in the center, a deeper, hotter layer is visible, resulting in a brighter appearance due to the higher temperatures.

Under high magnification, up to a few arcsec, the photosphere does not appear smooth; instead, it presents a fragmented appearance, known as *granulation*. This pattern features brighter parts termed *granules* surrounded by fainter parts known as *intergranular lanes*. This phenomenon is an effect of temperature difference arising from the convection zone beneath the photosphere, where hotter, inner material rises to the surface and cooler, outer material descends. This pattern is dynamic and undergoes renewal every 5-10 min. (Kutner, 2003)

3.5. Chromosphere

The optically thin layer directly above the photosphere is known as the chromosphere. It is usually overwhelmed by the brighter photosphere radiation in most parts of the spectrum, making it challenging to observe. However, it becomes visible just before and after a total solar eclipse, where the moon blocks radiation from the photosphere. Additionally, it can also be studied using a $H\alpha$ filter, where it emits a characteristically red glow due to the $H\alpha$ emission.

On the chromosphere, a large-scale pattern called *supergranulation* can be observed, also attributed to convective motion.

Spectroscopic observations during a total solar eclipse reveal a *flash spectrum*, allowing scientists to determine the chromosphere's temperature, estimated to be around 15000 K. However, the Sun does not seem that hot because of the low opacity of this layer. (Kutner, 2003)

3.6. Corona

The outermost and faintest part of the Sun is called corona, directly observable only during a total solar eclipse without the need for additional instruments. Otherwise, even a little fraction of scattered photospheric light can overwhelm the corona radiation and it can not be observed. Because total solar eclipses are rare, scientists developed a special telescope named the coronagraph, enabling the observation of the corona without an eclipse, although it remains sensitive to atmospheric scatter light. Addressing this issue

with a space coronagraph improves observations, but it is still not as good as during a total solar eclipse.

The appearance of the corona is very irregular, and the origin of its shape is still under investigation. Some studies suggest its form may be influenced by various solar events. Current corona models focus on three parts: the E-Corona, K-Corona, and F-Corona, distinguished by the processes believed responsible for each layer's light emission or scattering

Surprisingly, the corona has an even higher temperature than the chromosphere, reaching around 1-3 million K. The mechanisms driving this extreme heating remain the subject of ongoing research. Intuitively, events like coronal mass ejections should cool down by releasing huge amounts of energy into interplanetary space. (Kutner, 2003)

4. Solar Activity

In the following paragraph, different solar activity features will be discussed, some of which could significantly impact Earth, astronauts, and satellites in orbit.

4.1. Sunspots

Sunspots were discovered by Galileo in 1610 as dark patches on the solar surface. These spots appear dark because they are cooler compared to the surrounding material. As seen in Figure 4.1, a spot is separated into two parts. The colder center part is the *umbra* with a temperature of around 4300 K, surrounded by the *penumbra* with a temperature of about 5000 K. Sunspots have a finite lifetime depending on their size, ranging from only hours for small ones to weeks for larger spots or groups.

In the 1840s, Christian Horrebow recognized that sunspot activity seemed to vary periodically, and Schwabe (1844) later identified this variation known as the *solar cycle*. The solar cycle, approximately 11 years in length, spans from one solar activity minimum to the next; the current solar cycle is numbered 25, with its peak expected in 2025. The cycle exhibits an asymmetry to the maximum. At the beginning of a cycle, sunspots appear at higher latitudes, 20-25 degrees above and below the equator. As the cycle

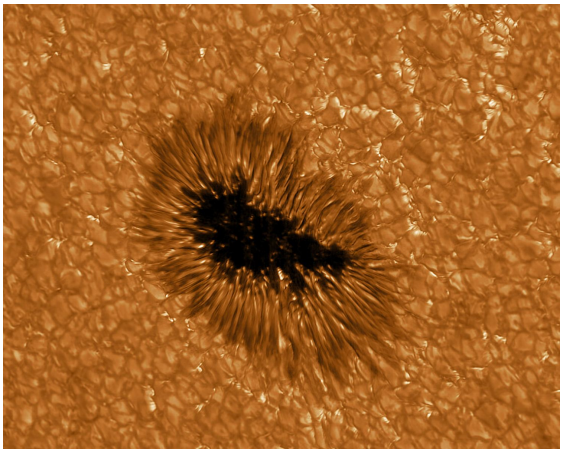

Figure 4.1.: The image captures a sunspot observed through the solar GREGOR Telescope in Spain. At its center, the colder umbra is surrounded by the penumbra. Additionally, the granulation effect on the photosphere is visible, showing the Sun's complex surface dynamics. (from Cimone, 2020)

advances, these spots drift towards the equator, though they never align precisely with it, a phenomenon known as *Spöerer's law*.

It has been known since Hale (1908) that sunspots tend to group in pairs that are connected via a strong magnetic field loop. In this pair, one spot acts as the preceding spot, and the other serves as the following spot with opposite magnetic polarity. Additionally, it has been observed that the preceding spot is located at a smaller distance to the equator than its following one, known as *Joy's law*.

Maunder (1904) illustrated all these sunspot behaviors in his famous *butterfly diagram*, shown in the upper part of Figure 4.2. The butterfly diagram plots the sunspot area as a function of latitude and time. Another interesting effect that can be seen in this diagram is that sunspots from a previous and following cycle overlap at the beginning of the new cycle.

Daily records of the solar surface are used to define the sunspot number (SN), which serves as an indicator of solar activity. It is a weighted number between sunspots and the number of spots in groups, calculated with Equation (4.1).

$$SN = k \cdot (10 \cdot g + s) \tag{4.1}$$

Here, k is a factor reflecting the quality of the used data, g represents the number of groups, and s is the number of sunspots. (Hathaway, 2015)

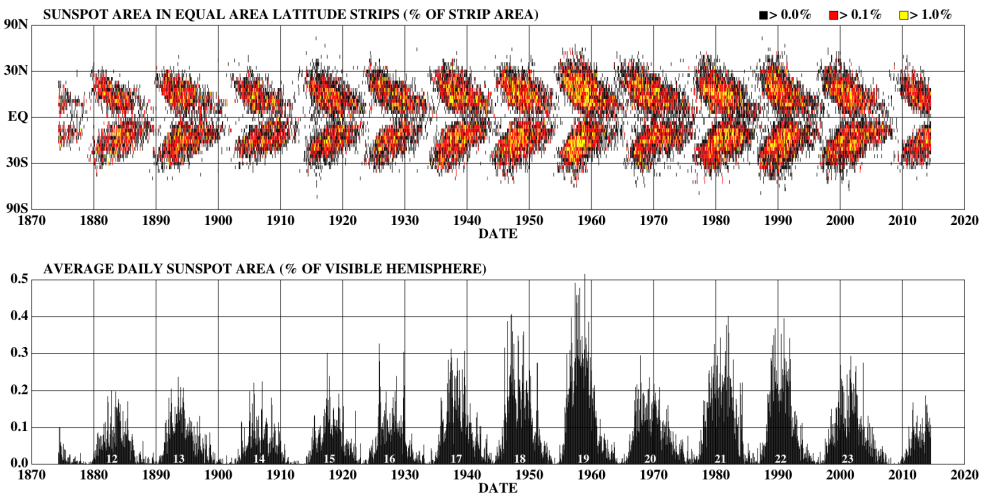

Figure 4.2.: The upper image presents a sunspot butterfly diagram, illustrating the characteristic butterfly pattern that comes from the equatorial drift of sunspot regions during the solar cycle. The color represents the fraction covered by sunspots, highlighting the distribution and density of sunspot activity. Additionally, this diagram captures the overlap of sunspots at the beginning of a new cycle. The lower plot details the average daily sunspot area, showing the solar cycle's asymmetry. (from Hathaway, 2015)

4.2. 10.7cm Solar Flux ($F_{10.7}$)

Besides the sunspot number, the 10.7 cm solar flux or $F_{10.7}$ is a widely used indicator for solar activity. This quantity corresponds to the flux density of the total emission at a wavelength of 10.7 cm or 2800 MHz with a bandwidth of 100 MHz, but by convention, it is often referred to as a flux. The choice of this specific wavelength was somewhat random. The first solar radio observations were made in 1945. By the 1940s, a connection between the sunspot number and the solar flux had already been discovered, but as Hathaway (2015) explained, the connection is non-linear, and the flux tends to lag behind the sunspot number for about a month. (Tapping, 2013)

4.3. Solar Wind

The solar wind is a constant flow of charged particles, comprising positive ions, and electrons into interplanetary space. It takes between 5-10 days to reach the Earth and impacts its magnetic field at a speed of 400-450 km/s. When the charged particles interact with the Earth's atmosphere, it results in an event known as *aurora*. This wind also interacts with particles from outside the solar system called cosmic rays. The flux of this particle stream varies with the level of solar activity. During periods of maximum solar activity, more and stronger aurora can be observed, even in lower latitudes, and fewer cosmic rays are detected in the Earth's atmosphere.

When the cosmic rays enter the Earth's atmosphere, they interact with ^{14}N and ^{16}O atoms, leading to the formation of new atoms and molecules. The newly created elements, e.g., ^{14}C, are oxidized to CO_2, which is then utilized by plants during photosynthesis. Thus, the new elements are deposited and become recognizable in plants. The deposited elements can also be used to reconstruct solar activity in the past, even before the first direct observations were recorded. The cosmic ray reduction typically lags behind the solar cycle by around 6-12 months and is anti-correlated. (Hathaway, 2015)

4.4. Solar Flares (SFs) and Coronal Mass Ejections (CMEs)

Solar flares (SFs) are solar events where a huge amount of energy in form of intense ultraviolet and X-ray emission is released into space. The first observation of a white light SF was reported by Carrington (1859) and Hodgson (1859) independently. Although solar flares only last a few minutes, they can have a significant impact on Earth by disrupting or even destroying satellites orbiting Earth. Flares are categorized based on the X-ray flux peak into A, B, C, M, and X flares. X and M- Flares exhibit the highest flux and pose the greatest risk to Earth, while A-C tends to have a smaller impact. Hathaway (2015) also notes that the X and M flares follow the solar cycle.

Coronal mass ejections (CMEs) are often linked with SF, although they can occur independently. CMEs are explosive emissions of plasma that carry the solar magnetic

field into space. Geomagnetic storms on Earth are often a consequence of CMEs on the Sun and similar to flares, CMEs are also influenced by the solar cycle.

Both phenomena are thought to result from magnetic reconnection within the solar interior, a process that releases a significant amount of energy. (Grodji et al., 2022)

4.5. Coronal Holes (CHs)

Coronal holes (CHs) are visible in X-ray images as darker regions on the solar corona, characterized by their reduced density and cooler temperatures compared to the surrounding areas. These regions are associated with *open* magnetic field lines that are connected to the high-speed solar wind. During the solar cycle minimum, CHs predominantly cover the regions at the pole caps. As the solar cycle progresses towards the maximum, the holes become more prevalent at lower latitudes on the solar disk. (Cranmer, 2009)

4.6. Prominences and Filaments

Prominences and filaments are the same solar phenomena, referred to by the location where they are observed. Prominences are seen as bright $H\alpha$ emissions at the solar limb, while filaments are dark $H\alpha$ absorption regions on the solar disk. Generally, these are regions in the lower corona where the density is much greater than the one from the surrounding area and are guided in a loop by the magnetic field. Prominences and filaments can have a lifetime of a few rotations, but it is somewhat unclear how they can be stable for that long because of gravitation and heating. When they are ejected and carry the magnetic field with them, they become CMEs. (Mackay, 2021)

4.7. Plages Regions

Plages are regions on the solar chromosphere found near active regions (ARs) like sunspots. They have a strong, prominent Ca II H and K spectral line. These regions are seen as bright zones due to the higher temperature than the rest of the chromospheric matter. Current theories are that the higher temperatures come from magnetic energy transport and ARs in this area. The fact that plages persist after the disappearance of sunspots also makes them interesting objects of solar research. (Santos et al., 2023)

5. Solar Rotation Observation

5.1. History

Before Galileo discovered sunspots in 1610, it was believed that the Sun was a perfect sphere without any marks. About 20 years later, Christoph Scheiner (1630) noted that sunspots near the equator crossed the solar disk faster than those near the poles; this was the first-ever observation of solar differential rotation. (Arlt et al., 2016)

The following sections will discuss and compare the different techniques used for observing the solar differential rotation. Therefore, it is essential to use the correct coordinate system. Most of the time, Carrington's (1863) heliographic longitude L and latitude B are used. In this system, the rotation rate Ω as a function of latitude B is expressed in the form seen in Equation (5.1).

$$\Omega(B) = a + b \cdot \sin^2(B) + c \cdot \sin^4(B) \tag{5.1}$$

Here, a is the equatorial rotation rate, while b and c are factors that set the differential rate. Conventionally, the power of the sine expressions is even. However, it can also be the case that the factor c is set to zero because the method to measure the rotation does not provide full latitude coverage. (Beck, 2000)

5.1.1. Tracer Motion

To obtain the solar rotation from tracers like sunspots, the simple Equation (5.2) is used:

$$\Omega(B) = \frac{L_2(B) - L_1(B)}{t_2 - t_1} = \frac{\Delta L(B)}{\Delta t} \tag{5.2}$$

Here, the angular displacement ΔL is divided by the time difference Δt between the measurements. If the measurements are taken at different latitudes, they can be fitted by a function as shown in Equation (5.1). (Beck, 2000)

Carrington (1863) made the first quantitative observation of the differential rotation by measuring the movement of thousands of sunspots in the years 1853 to 1861. This led to his famous finding that the rotation rate Ω varies with latitude B with, $\Omega(B) \approx \sin^{7/4}(B)\, deg\, d^{-1}$. The most important work on sunspots as tracers was made by Newton and Nunn (1951), who fitted a rotation behavior of

$$\Omega(B) = 14.38 - 2.96 \cdot \sin^2(B)\, deg\, d^{-1}$$

using sunspot observations from six different solar cycles between 1878 and 1944.

5.1.2. Spectroscopy

In the early 20th century, advancements in spectroscopy were utilized to determine solar rotation (e.g. Adams, 1909). The simplest method involves measuring the Doppler shifts $\Delta\lambda$ on the western and eastern limbs of the Sun. These $\Delta\lambda$ values can be used in the Doppler effect Equation (2.2) to calculate the radial velocity v_r. Knowing the radius r at the observed latitude B enables the calculation of the rotation rate by using Equation(5.3).

$$\Omega(B) = \frac{v_r(B)}{r} \tag{5.3}$$

If this process is repeated for different latitudes, the data points can then again be used to derive a function for the rotation rate $\Omega(B)$. (Gill, 2012) The most cited work on spectroscopic observation where made by Howard and Harvey (1970). They obtained a rotation curve of

$$\Omega(B) = 13.76 - 1.75 \cdot \sin^2(B) - 2.9 \cdot \sin^4(B)\, deg\, d^{-1}$$

by analyzing data from 1966 to 1968. Other features have also been used for spectroscopic observations in the past. Glackin (1974) used filaments and prominences, Belvedere et al. (1977) used solar plages, Oghrapishvili et al. (2018) used coronal holes, and the most recent studies use coronal bright points (CBPs)(e.g. Sudar et al., 2015).

5.1.3. Helioseismology

Helioseismology was a groundbreaking milestone in solar physics in the 1980s. This innovative technique involves the observation of pressure mode, or *p-mode*, frequencies, which are standing sound waves generated within the inner solar layers. As these p-modes travel through the solar interior, they induce oscillations on the solar surface due to reflection on its inner boundary and carry out critical information about the interior and dynamics. Key discoveries with helioseismology include the detailed description of the internal solar structure and the reveal of the complex internal rotation profile, which varies with latitude and depth.

Every p-mode is characterized by its spherical harmonic indices, n as the radial order, l as the angular degree, and m as the azimuthal order. Here, it is important to note that m ranges from $-l$ to l. These modes depend on the cyclic frequency ν_{nlm}. If the star is rotating, this frequency depends on m, resulting in a frequency difference $\Delta\nu_{nlm} = (\nu_{nl+m} - \nu_{nl-m})$. With the rotation profile Equation 5.4, where r is the distance from the center, K_{nlm} represents mode kernels, and B is the latitude, the rotation curve at various depths, $\Omega(r, B)$, can be determined by rearranging. (Beck, 2000)

$$\Delta\nu_{nlm} = \int\int K_{nlm}(r, B)\Omega(r, B) r\, dr dB \tag{5.4}$$

5.1.4. Comparison

From the above results, it can be seen that the rotation rates differ with the different methods. The rate obtained from sunspots by Newton and Nunn (1951) is significantly

higher than the rate from Howard and Harvey (1970) using spectroscopy. Beck (2000) compared the different methods and he showed that the rotation rate is dependent on the feature. Sunspots and other tracers possess an *anchor depth* because they rotate faster than the surface rotation determined by helioseismology investigations. Moreover, Beck's findings suggest that the rotation rate of sunspots is also age-dependent; younger sunspots correspond to a rotation rate at approximately $0.93R_\odot$, while older spots suggest even deeper anchor depths.

5.2. Current State

As Kitchatinov (2011) outlines, the current theory of differential rotation includes three different observable parts: the differential rotation itself, the differential temperature, and the meridional flow. These parts will be discussed in detail in this section. They are interconnected and play a critical role in the framework of the solar dynamo theory, a topic discussed in Chapter 6.

5.2.1. Differential Rotation

Global helioseismology observations have inferred that the origin of the differential rotation is a thin shear layer called the *tachocline* between $0.66R_\odot$ to $0.73R_\odot$. The differential rotation has the characteristic that the equator rotates about 30% faster than the poles. In the inner region of the convective zone, the rotation rate varies highly with the latitude but not with the radius. The outermost layer is called the *near-surface shear layer*, where the rotation rate drops about 5% at all latitudes due to the shear. These effects are illustrated in Figure 5.1. It shows results from helioseismic observations made by the Global Oscillation Network Group (GONG) and the Helioseismic and Magnetic Imager (HMI). (Hotta et al., 2022)

Theories used to describe this differential rotation focused on the interaction between thermal convection and the Coriolis force. Due to the high Reynolds number R_e, convection within the solar interior becomes turbulent. The inclusion of the Coriolis force, which changes with latitude, introduces anisotropy into the turbulent flow. The Coriolis force has a stronger impact on the plasma at the poles compared to the equator, causing the plasma in the polar regions to decelerate. This variation in deceleration across different latitudes is believed to be the reason for the solar differential rotation. (Hotta et al., 2023)

The differential rotation profile can be influenced by *torsional oscillations*, which are bands aligned along the latitudes that are either slower or faster than the average rotation rate. The faster bands move from mid-latitudes to the equator from one solar cycle minimum to the next. It has also been observed that the solar rotation rate accelerates before a major solar activity event. (Norton et al., 2023)

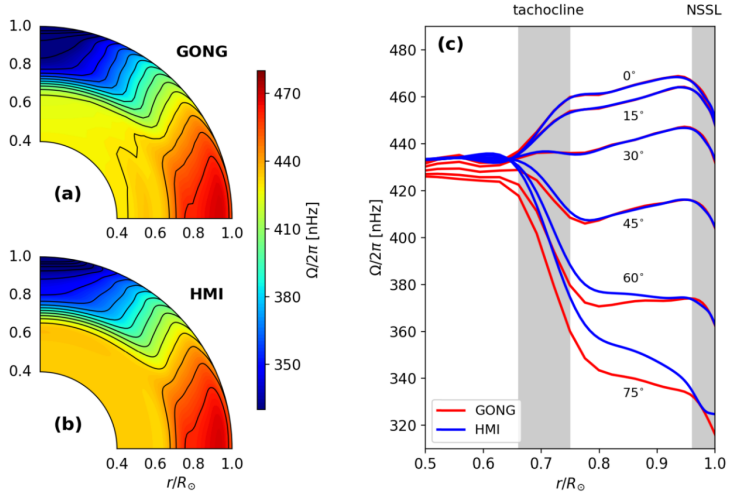

Figure 5.1.: The left images (a) and (b) display the outcomes of rotation measurements conducted by the Global Oscillation Network Group (GONG) and the Helioseismic Magnetic Imager (HMI) aboard the Solar Dynamics Observatory (SDO). In both plots, it is evident that the core rotates uniformly while the outer layers exhibit differential rotation. In panel (c), the rotation profile of the solar interior is plotted, with gray shades highlighting the two significant shear layers: the tachocline and the near-surface shear layer (NSSL). (from Hotta et al., 2023)

5.2.2. Meridional Flow

The interplay of the differential rotation with the observable temperature difference of about 2.5 K between the poles and the equator, known as *differential temperature*, leads to a circulation from the equator to the poles. (Rast et al., 2008)

This large-scale circulation, known as *meridional flow* in the solar context, can be theoretically explained by two primary hydrodynamic mechanisms: *centrifugal driving* and *baroclinic driving*. The first driving is present due to the effect of differential rotation because it is sensitive to angular velocity variations that depend on the distance from the center. This effect generates a torque leading in a counter-clockwise circulation, as illustrated in the left part of Figure 5.2. The baroclinic driving acts against the centrifugal driving. With the ideal gas law, the connection between density ρ and temperature T can be derived, resulting in $\rho \propto 1/T$. Due to the differential temperature mentioned above, material at lower latitudes, being cooler and denser, tends to sink inwards. On the other hand, material near the poles, which is warmer and less dense, rises outwards and spreads over the solar surface. This generates a clockwise flow, as shown on the right side in Figure 5.2. (Kitchatinov, 2013)

These two effects are nearly equal in solar-like stars and can be expressed in the *thermal wind balance*. However, a slow circulation of an amplitude of approximately $10 - 20ms^{-1}$

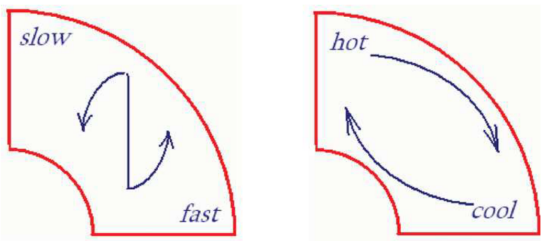

Figure 5.2.: The illustration showcases the two primary hydrodynamic mechanisms responsible for the observable meridional flow from the solar equator to the poles. On the left, the counter-clockwise centrifugal driving is sketched, resulting from differential rotation. The right image illustrates the counter-clockwise baroclinic driving, which occurs due to differential temperature. (from Kitchatinov, 2013)

from the equator to the poles can be maintained and observed. This flow is among the most challenging ones to observe within the solar interior, as it is a few orders weaker than both the differential rotation and convective motion. Studies on the meridian flow have shown that it is correlated with the solar cycle.

This flow must fulfill the mass conservation, implying a return flow to the equator is needed. Either a single-cell or double-cell motion in each hemisphere could do this, but more research is needed to determine which represents the reality. Despite not being fully understood, the meridional flow has become an important aspect of the Babcock-Leighton model in the solar dynamo theory. (Norton et al., 2023)

6. Dynamo Theory

6.1. Observational Effects

Hale (1908) discovered the magnetic field in sunspots and also demonstrated these are commonly observed in pairs with opposite polarity on the solar surface. All preceding (or leading) spots exhibit the same polarity on one hemisphere and the opposite polarity on the other. This polarity pattern changes during the 11-year solar cycle, which defines a 22-year magnetic cycle. This phenomenon, known as *Hale's law* is illustrated in the *magnetic butterfly diagram* in Figure 6.1 similar to the Maunder butterfly diagram in Figure 4.2. The solar dynamo theory aims to explain how the Sun generates and maintains its magnetic field and to link it to solar activity and the (magnetic) solar cycle.

6.2. Theory

The key equation to describe the dynamics of the solar magnetic field is the induction Equation of magnetohydrodynamics (MHD)(6.1). It explains how the magnetic field in a conducting fluid, like plasma, evolves.

$$\frac{\partial \boldsymbol{B}}{\partial t} = \underbrace{\eta \nabla^2 \boldsymbol{B}}_{\text{diffusion}} + \underbrace{\nabla \times (\boldsymbol{u} \times \boldsymbol{B})}_{\text{advection}} \tag{6.1}$$

In this equation, $\boldsymbol{B}$ is the magnetic field, η is the magnetic diffusivity, and $\boldsymbol{u}$ is the fluid velocity. The equation has two different terms: the first term is the diffusion term produced by the conductivity of the fluid, while the second is an advection term coming from the plasma velocity. The advection term is responsible for stretching, twisting, or folding magnetic field lines.

If it is assumed that the terms share the same scale length L that $\nabla L \approx 1/L$ and scale velocity $U \approx \boldsymbol{u}$, they can be written as:

$$\eta \nabla^2 \boldsymbol{B} \approx \frac{\eta B}{L^2}$$

$$\nabla \times (\boldsymbol{u} \times \boldsymbol{B}) \approx \frac{UB}{L}$$

By taking the ratio of these two terms, the importance of advection against diffusion by the conductivity of the fluid can be found. This dimensionless parameter is the *Magnetic Reynolds number* R_m in Equation (6.2).

$$R_m = \frac{\text{advection}}{\text{diffusion}} = \frac{UL}{\eta} \tag{6.2}$$

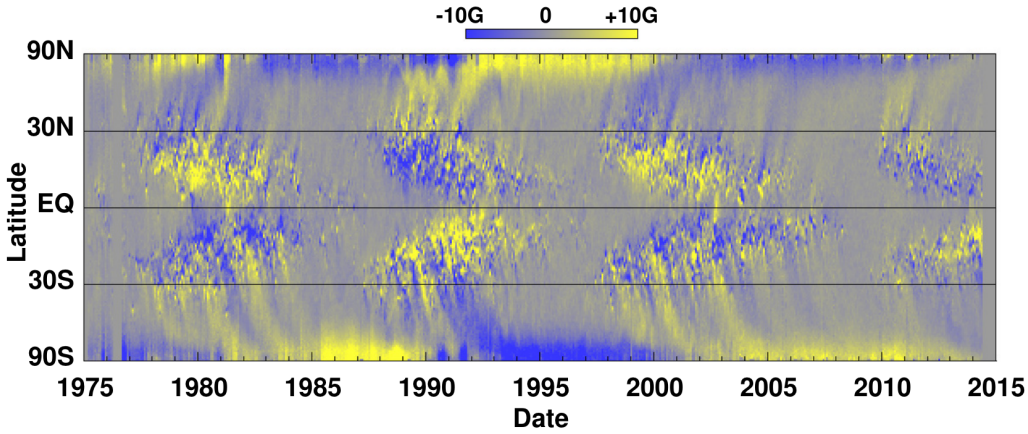

Figure 6.1.: The magnetic butterfly diagram plots sunspot latitudes against observed time, with different colors representing the averaged radial magnetic field polarity of the spots, as observed with the Kitt Peak and SOHO instruments. This diagram illustrates Hale's Polarity Law, polar field reversal, the equatorial drift (Joy's Law), and the 22-year magnetic cycle, providing a comprehensive visual representation of these fundamental solar phenomena. (from Hathaway, 2015)

The advection term becomes large at the tachocline region due to the high shear flow U and significant large-scale length L. On the other hand, the magnetic diffusion η is low because of the solar plasma's high electric conductivity σ. Resulting in a large $R_m \gg 1$ means the magnetic field is advection dominated, so *Alfvén's theorem* or *frozen-in theorem* holds, leading to magnetic field lines following the solar plasma motion. (Hood and Hughes, 2011)

6.2.1. Ω-Effect

Alfvén's theorem and differential rotation combine to the Ω-effect in the solar dynamo theory. This effect begins with a primordial poloidal magnetic field that undergoes significant transformation under the influence of solar differential rotation. The faster equatorial rotation twists the magnetic field lines, converting the original poloidal field into a toroidal one aligned along the solar latitudinal axis. This phenomenon is visualized in the first part of Figure 6.2 for a better understanding. This mechanism is well understood, but it is crucial that there is a reversal process to maintain the solar magnetic dynamics. Current research focuses on two main concepts explaining the back transformation to a poloidal field. The first one is the *α-effect* by Parker, and the other is known as the *Babcock-Leighthon model*. Both mechanisms are explained in the next sections. (Sanchez et al., 2013)

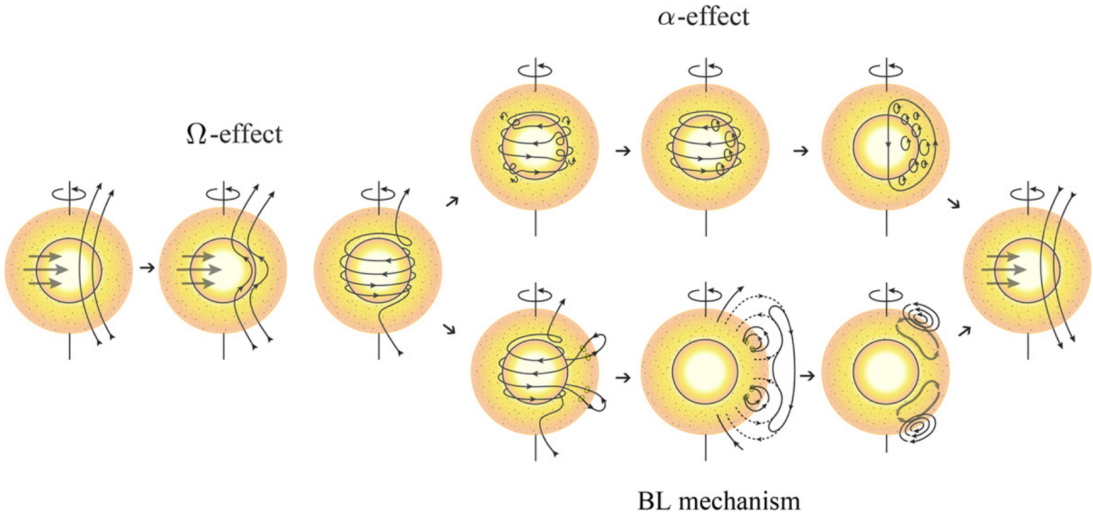

Figure 6.2.: The left part of the illustration visualizes the Ω-effect, responsible for transforming the magnetic field from a poloidal configuration into a toroidal one. On the right, the two leading theories for reversing this process are shown; the upper segment introduces the α-effect, as proposed by Parker, where cyclic turbulences are crucial. The lower segment presents the Babcock-Leighton (BL) model, which accounts for magnetic buoyancy and the meridional flow as key mechanisms. (from Sanchez et al., 2013)

6.2.2. α-Effect

Parker (1955) developed the mean α-effect based on cyclic turbulence in the convection zone. This turbulence acts on the toroidal field lines, leading to the twisting of the magnetic field lines. During this twisting, magnetic field lines with opposite polarity approach each other, and a small magnetic pole loop can be detached due to the effect of magnetic reconnection. As illustrated in the upper right part of Figure 6.2, combining many small poloidal loops at various latitudes results in a large-scale poloidal magnetic field, and the process begins again at the Ω-effect.

6.2.3. Babcock–Leighton Model

Magnetic buoyancy plays a critical role in the Babcock–Leighton model (BL)—shown in the lower part of Figure 6.2. It can be seen as an extension of the α-effect or a standalone model for the solar magnetic dynamics.

Due to the pressure difference between the inside of the magnetic flux tube and the surrounding convective zone pressure, the flux tube experiences a buoyancy force (magnetic buoyancy force) toward the outside. This raises the flux tube through the photosphere, where it manifests as a sunspot pair. The strong magnetic field within the sunspots

suppresses the convective energy transport in this area, resulting in a lower temperature compared to the rest of the photosphere; the spots appear darker. The rising tube also explains the observed polarity difference because it exits the photosphere in one spot and re-enters it in the other. If the Coriolis force is considered, the following spot experiences a drift toward the pole, explaining the tilt between the spots (Joy's law). In the BL model, the decaying magnetic field of the sunspots is transported toward the poles by the meridional flow, which explains the polarity change during the magnetic solar cycle and the transformation into a poloidal field. (Babcock, 1961),(Leighton, 1969)

To completely understand the solar dynamo, some research with numerical simulations is still needed, as Charbonneau and Sokoloff (2023) pointed out in their work. The general features of solar activity phenomena and their connection to the magnetic field are already analyzed in Chapter 4. For completeness, I will repeat their connection to the magnetic field.

- Sunspots are associated with rising magnetic flux tubes due to a magnetic buoyancy force.
- Flares and CMEs are short events that occur because of large-scale magnetic reconnection.
- Coronal holes are observed in corona regions with *open* magnetic field lines, and these holes are connected to high-speed solar wind.
- Prominences are denser and colder plasma loops that are located at the solar limb and shaped by the magnetic field.

7. Sunspots as Tracers

In the last part of my thesis, I used the same method as Carrington (1863) or Newton and Nunn (1951) discussed in Section 5.1.1 to analyze the differential rotation of sunspots. I utilized images from the Solar Dynamics Observatory (SDO), which is a NASA space mission launched in 2010, aimed at understanding the impact of the Sun and space weather on Earth. It is capable of observing the solar atmosphere in a wide wavelength range simultaneously. For my analysis, I used images from the Helioseismic Magnetic Imager (HMI); this instrument captures an image of the solar surface every 45 seconds in a narrow region in the visible light around 6173Å. At this wavelength, the sunspots are clearly visible. (NASA)

7.1. Method

7.1.1. Image Processing

I wrote a Python script that automatically tracks the sunspots over time to obtain the most accurate result. I discovered the Python package *cv2*; this tool can be used for image analysis and face/object tracking.

Using the Python package *sunpy*, I first downloaded the required FITS files for the days between 23.11.23 and 04.12.23. I chose these days because I knew the sunspot coverage was high, but I could also use the sunspot number from Section 4.1 to find a date with high coverage. The Python code used to download the FITS files can be found in the Appendix A. Article from DZdata.com (2023) inspired the image processing approach I used to detect spots in the images.

The processing is done in three steps:

1. Applying a *Gaussian blur filter* to reduce the noise
2. Implementing an *inverse adaptive Gaussian threshold* to binarize the image, which means the region of dark sunspots becomes white pixels and the others black, illustrated in Figure 7.1(a)
3. Lastly, the use of the *dilate and erode* commands closes smaller holes and errors in the regions

After this reduction process, I used the command *connectedComponentsWithStats*, a powerful command from the cv2 package that labels the connected region in the binary image; this is also known as *Connected-component labeling (CCL)*. The results of the

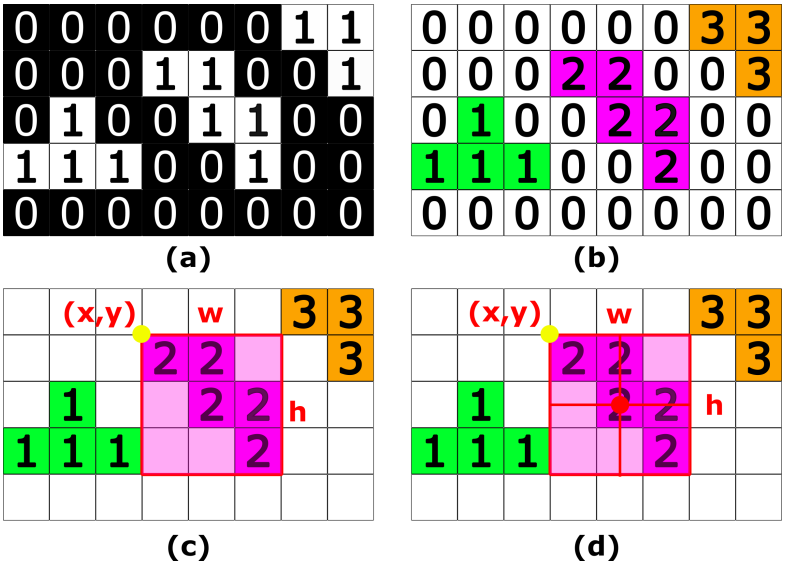

Figure 7.1.: The illustration details the various steps of the image processing utilized to identify sunspots and their midpoints in the image. In (a), the binarized image required for the Connected-Component Labeling (CCL) process, shown in (b), is presented. Panel (c) illustrates the parameters resulting from the merging process, while (d) demonstrates how the midpoint is determined from these parameters.

CCL included the top left corner locations of the spots (x, y), the areas of the connected components, the widths w, and the heights h in pixels, as seen in Figure 7.1(c).

In the next step, I use the areas to filter out regions too small to track, as well as the largest area corresponding to the whole solar disk. I also exclude spots not within $0.8r_{\odot}$ of the solar center because spots near the eastern limb could be lost during later tracking, making them unhelpful for the calculation. The final step before tracking involves using the Euclidean distance between spots to group them if their separation falls below a specified minimum distance.

The tracking command requires an initial position box around the spots to initiate tracking; this was achieved by applying the previously described image processing to the first image in the series.

The image series consists of 72 FITS files with a spacing of 1 h, representing a total of three days. The series was then visualized with the tracking for a final check so I could decide whether or not to keep the spot as a tracer because it is possible that the tracking field would be lost if it disappeared or merged with other spots. If I thought the spot was a good candidate for the calculation, the script saved its start (x_1, y_1) and end position (x_2, y_2) as well as the time difference Δt. The positions were calculated from the

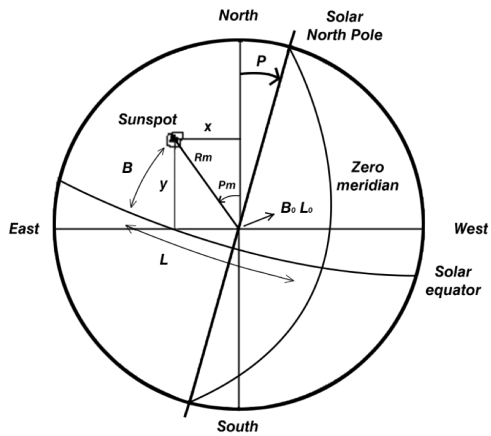

Figure 7.2.: The Carrington heliographic coordinate system (HGC) is one of the two main systems used to define points on the solar surface with longitude L and latitude B. The two systems are only different in their definition of longitude. In the HGC, the zero meridian rotates with a period of ≈ 27.257 days. The angle P is the tilt of the solar rotation axis. (from ESA)

boxes around the spot at the start and end point with Equation (7.1), this process is also illustrated in Figure 7.1(d). The Python code used to detect and track the sunspots can be found in Appendix B.

$$(x_n, y_n) = (x + w/2, y + h/2) \tag{7.1}$$

7.1.2. Calculation of the Rotation Rate

To calculate the rotation rate, I utilized the equation already described in Section 5.1.1, which I will repeat for completeness in Equation (7.2). Here, ΔL represents the difference in the Carrington heliographic longitude on the solar surface, and Δt is the time that separates the two measuring points.

$$\Omega = \frac{\Delta L}{\Delta t} \tag{7.2}$$

The Carrington heliographic coordinate system (HGC) is shown in Figure 7.2. This system is mainly used to track features on the solar surface over a longer time. Its zero point is located at the center of the Sun. It is a rotating system invented by Carrington (1863) with an imaginary zero meridian between the north and south poles that rotates with a period of ≈ 27.257 days. The transformation from pixel values to HGC longitude and latitude is very complex, so I took advantage of the FITS file format. The header contains all the information needed to automatically convert the coordinates with the *astropy* and *sunpy* packages. After the transformation, I plotted the position of the tracked points over the first and last image, as seen in Figure 7.3, to check if the transformation was

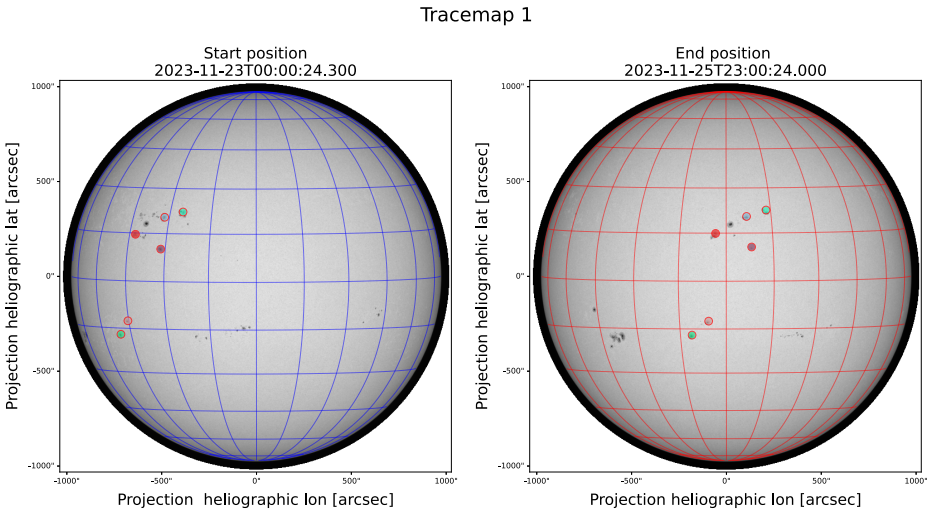

Figure 7.3.: On the left side, the initial position of the spots is displayed, while the right side shows their final position, with the images being separated by a time interval of $\Delta t = 72$ hours. The x and y axes feature the projection of the heliographic coordinates, and the grid represents the Carrington heliographic coordinate system.

successful. In the next step, I calculated the start and end position longitude difference ΔL to use it in Equation (7.2) with the time difference Δt between the two measurements. Equation (7.3) provides the needed transformation from the rotation rate to the period P in *days*. $\Omega(B)$ must be expressed in the correct unit of $deg\, d^{-1}$.

$$P = \frac{360\, deg}{\Omega} \tag{7.3}$$

To illustrate the final result in a plot, I plotted the HGC latitude B against the period P. Given that the latitude also changes slightly over time, I calculated the absolute mean of the start and end latitude for the plot. To fit the data point, I used a function in the form of Equation(7.4), which represents the commonly used form to express the solar differential rotation.

$$\Omega(B) = a + b \cdot \sin^2(B) \tag{7.4}$$

Here, a is the equator rotation rate, and b is the factor that represents the application of the differential rotation with the latitude. Also, the calculation code can be found in Appendix C.

7.2. Result

Figure 7.4 shows the result, including the fitting function to the sunspot measurements. The x-axis represents the heliographic latitude in deg, and the period is marked on the

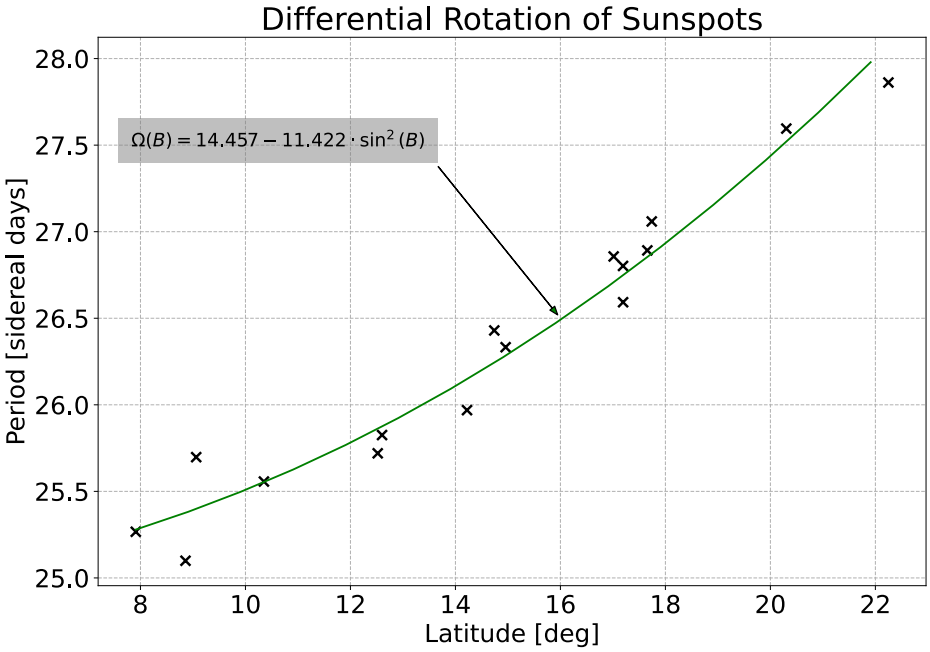

Figure 7.4.: This plot displays the mean Carrington heliographic latitude in degrees against its calculated period in sidereal days, illustrating the differential rotation of the sunspots. Sunspots are measured only between 8-23 degrees, a range known as Spöerer's law.

y-axis in sidereal days. The fitted values are:

$$a = 14.457\, deg\, d^{-1}$$

$$b = -11.422\, deg\, d^{-1}$$

The R^2-value of the fit is around 0.9576.

7.3. Discussion

The resulting plot in Figure 7.4 showcases the differential rotation of sunspots at various latitudes, confirmed by the very good R^2-value of the fit function. Spöerer's law can also be extracted, which means that sunspots can only be found until latitudes of 23 degrees. Comparing this latitude range with the butterfly diagram in Figure 4.2, it is evident that we are nearing the solar cycle maximum, expected in 2025.

From the fit values, an equatorial period of around 24.9 days seems plausible, aligning with other studies that utilized the same method, e.g., Newton and Nunn (1951) who reported an equatorial period of ≈ 25 days. I also noted two outliers at a latitude of ≈ 9 degrees, for which I have three different possible explanations:

1. The latitude drift of the two spots was significantly different from the others, leading to a left-right drift in the plot.
2. The initial position of the tracked spot was too close to the limb, and due to the projection, it is significantly stretched, so it is hard for the Python script to find and track the accurate midpoint.
3. As mentioned in Section 5.1.4, the sunspots seem to have an age dependency; older ones rotate faster than younger ones, which leads to an upward and downward movement in the graph.

8. Conclusion

With this thesis, I have provided a comprehensive insight into the connection between the solar differential rotation and the dynamo theory as well as the resulting solar activity. Starting with the exploration of the different layers of the Sun, revealing that a thin layer called tachocline appears to be very interesting in regards to the differential rotation. This layer is located between the radiative and convective zones.

In this region, the interaction between turbulence in the convective motion and the Coriolis force is believed to result in differential rotation that Scheiner observed while monitoring sunspots. These observations have evolved from the initial simple tracing methods, through spectroscopic techniques, to today's helioseismic observations. Helioseismology has revolutionized our understanding of the solar interior and rotational dynamics, introducing a new perspective on the rotational behaviors of the solar interior. Furthermore, it has revealed that the rotation rate depends on the observed feature and the observing technique used, a concept referred to as anchor depth.

With the Ω-effect of the dynamo theory, a direct connection between the differential rotation and magnetic dynamics is established. This well-understood Ω-effect requires a reversal process to maintain the dynamo mechanism. However, further research is necessary to determine whether the α-effect, the Babcock-Leighton model, or a combination of both accurately represent reality. While the Babcock-Leighton model can explain the rise and decay of sunspots, many other solar activity phenomena like CMEs, coronal holes, or prominences, which are deeply interconnected with the magnetic field, remain to be fully explained. Advancements in our understanding of differential rotation and magnetic dynamics promise to enhance current theories, offering deeper insights into the mechanisms driving the solar cycle. Hopefully, explaining how solar activity events evolve and help make predictions about them, reducing their negative impact on Earth.

And finally, with the empirical analysis of sunspots, the differential rotation was shown, offering results that align accurately with other studies. Additionally, two outliers in the dataset were identified that could be attributed to the age dependence of sunspots or the extreme stretching at the solar limb due to the projection effects. However, accuracy could be enhanced by tracking the sunspots over a longer time than three days or by refining the tracking method. Furthermore, the variable nature of sunspots makes it more complicated to track them. For future works, using images in a different wavelength and tracking another solar activity feature could offer new insights. This would be possible with a few adjustments to my script. Overall, the result shows the differential rotation as expected, and I am satisfied with it.

Bibliography

a-levelphysicstutor.com. Doppler effect 02. https://a-levelphysicstutor.com/images/waves/dopp-redshift03.jpg.

Walter S. Adams. Spectroscopic Investigations of the Rotation of the Sun during the Year 1908. *The Astrophysical Journal*, 29:110, March 1909. ISSN 0004-637X. doi: 10.1086/141635.

R. Arlt, V. Senthamizh Pavai, C. Schmiel, and F. Spada. Sunspot positions, areas, and group tilt angles for 1611-1631 from observations by Christoph Scheiner. *Astronomy & Astrophysics*, 595:A104, November 2016. ISSN 0004-6361, 1432-0746. doi: 10.1051/0004-6361/201629000.

H. W. Babcock. The Topology of the Sun's Magnetic Field and the 22-Year Cycle. *The Astrophysical Journal*, 133:572, March 1961. ISSN 0004-637X. doi: 10.1086/147060.

John N. Bahcall and Raymond Davis. Solar Neutrinos: A Scientific Puzzle. *Science*, 191 (4224):264–267, 1976. ISSN 0036-8075.

John G. Beck. A comparison of differential rotation measurements - (Invited Review). *Solar Physics*, 191:47–70, January 2000. ISSN 0038-0938. doi: 10.1023/A:1005226402796.

G. Belvedere, G. Godoli, S. Motta, L. Paterno, and R. A. Zappala. K faculae as tracers of the solar differential rotation. *The Astrophysical Journal*, 214:L91–L95, June 1977. ISSN 0004-637X. doi: 10.1086/182449.

R. C. Carrington. Description of a Singular Appearance seen in the Sun on September 1, 1859. *Monthly Notices of the Royal Astronomical Society*, 20:13–15, November 1859. ISSN 0035-8711. doi: 10.1093/mnras/20.1.13.

Richard Christopher Carrington. *Observations of the Spots on the Sun: From November 9, 1853, to March 24, 1861, Made at Redhill*. January 1863.

Paul Charbonneau and Dmitry Sokoloff. Evolution of Solar and Stellar Dynamo Theory. *Space Science Reviews*, 219(5):35, June 2023. ISSN 1572-9672. doi: 10.1007/s11214-023-00980-0.

Matthew Cimone. A Sunspot, Revealed in Incredible Detail by Europe's Newly Upgraded GREGOR Telescope, September 2020.

Steven R. Cranmer. Coronal Holes. *Living Reviews in Solar Physics*, 6(1):3, September 2009. ISSN 1614-4961. doi: 10.12942/lrsp-2009-3.

DZdata.com. How to Use Connected Components to Find Sunspots. https://dzdata.medium.com/how-to-use-canny-edge-detector-to-find-sunspots-b82047bab051, July 2023.

ESA. CESAR Science Case – Rotation period of the Sun and the sunspot activity. https://www.cosmos.esa.int/documents/519784/1185728/diff_rot_teachers_guide_pdf/50a35ee0-5912-4627-b0b1-3a11ef935f3e.

ESO. Sun layers. https://www.eso.org/public/outreach/eduoff/vt-2004/mt-2003/mt-2003-sun-interior-normal.jpg.

Robert M. Gill. The Rotational Period of the Sun Using the Doppler Shift of the Hydrogen alpha Spectral Line. *Society for Astronomical Sciences Annual Symposium*, 31:225–227, May 2012.

David L. Glackin. Differential Rotation of Solar Filaments. *Solar Physics*, 36:51–60, May 1974. ISSN 0038-0938. doi: 10.1007/BF00151542.

Oswald Didier Franck Grodji, Vafi Doumbia, Paul Obiakara Amaechi, Christine Amory-Mazaudier, Kouassi N'guessan, Kassamba Abdel Aziz Diaby, Tuo Zie, and Kouadio Boka. A Study of Solar Flare Effects on the Geomagnetic Field Components during Solar Cycles 23 and 24. *Atmosphere*, 13(1):69, January 2022. ISSN 2073-4433. doi: 10.3390/atmos13010069.

George E. Hale. On the Probable Existence of a Magnetic Field in Sun-Spots. *The Astrophysical Journal*, 28:315, November 1908. ISSN 0004-637X. doi: 10.1086/141602.

David H. Hathaway. The Solar Cycle. *Living Reviews in Solar Physics*, 12(1):4, September 2015. ISSN 1614-4961. doi: 10.1007/lrsp-2015-4.

R. Hodgson. On a curious Appearance seen in the Sun. *Monthly Notices of the Royal Astronomical Society*, 20:15–16, November 1859. ISSN 0035-8711. doi: 10.1093/mnras/20.1.15.

Alan W. Hood and David W. Hughes. Solar Magnetic Fields. *Physics of the Earth and Planetary Interiors*, 187(3-4):78–91, August 2011. ISSN 00319201. doi: 10.1016/j.pepi.2011.04.010.

H. Hotta, K. Kusano, and R. Shimada. Generation of Solar-like Differential Rotation. *The Astrophysical Journal*, 933:199, July 2022. ISSN 0004-637X. doi: 10.3847/1538-4357/ac7395.

Hideyuki Hotta, Yuto Bekki, Laurent Gizon, Quentin Noraz, and Mark Rast. Dynamics of Large-Scale Solar Flows. *Space Science Reviews*, 219(8):77, November 2023. ISSN 1572-9672. doi: 10.1007/s11214-023-01021-6.

Robert Howard and J. Harvey. Spectroscopic determinations of solar rotation. *Solar Physics*, 12(1):23–51, April 1970. ISSN 0038-0938, 1573-093X. doi: 10.1007/BF02276562.

L. L. Kitchatinov. Solar differential rotation: Origin, models and implications for dynamo. 2:71–80, January 2011. doi: 10.48550/arXiv.1108.1604.

Leonid L. Kitchatinov. Theory of differential rotation and meridional circulation. 294: 399–410, July 2013. doi: 10.1017/S1743921313002834.

Marc L. Kutner. *Astronomy: A Physical Perspective*. Cambridge University Press, July 2003. ISBN 9780511802195. doi: 10.1017/CBO9780511802195.

Robert B. Leighton. A Magneto-Kinematic Model of the Solar Cycle. *The Astrophysical Journal*, 156:1, April 1969. ISSN 0004-637X. doi: 10.1086/149943.

Duncan Hendry Mackay. Solar prominences. Oxford University Press, February 2021. ISBN 978-0-19-087199-4.

E. Walter Maunder. Note on the Distribution of Sun-spots in Heliographic Latitude, 1874-1902. *Monthly Notices of the Royal Astronomical Society*, 64:747–761, June 1904. ISSN 0035-8711. doi: 10.1093/mnras/64.8.747.

NASA. SDO | Solar Dynamics Observatory. https://sdo.gsfc.nasa.gov/.

H. W. Newton and M. L. Nunn. The Sun's Rotation Derived from Sunspots 1934–1944 and Additional Results. *Monthly Notices of the Royal Astronomical Society*, 111(4): 413–421, August 1951. ISSN 0035-8711. doi: 10.1093/mnras/111.4.413.

Aimee Norton, Rachel Howe, Lisa Upton, and Ilya Usoskin. Solar Cycle Observations. *Space Science Reviews*, 219(8):64, October 2023. ISSN 1572-9672. doi: 10.1007/s11214-023-01008-3.

N.B. Oghrapishvili, S.R. Bagashvili, D.A. Maghradze, T.Z. Gachechiladze, D.R. Japaridze, B.M. Shergelashvili, T.G. Mdzinarishvili, and B.B. Chargeishvili. Study of the solar coronal hole rotation. *Advances in Space Research*, 61(12):3039–3050, June 2018. ISSN 02731177. doi: 10.1016/j.asr.2018.03.033.

Eugene N. Parker. Hydromagnetic Dynamo Models. *The Astrophysical Journal*, 122:293, September 1955. ISSN 0004-637X. doi: 10.1086/146087.

Mark P. Rast, Ada Ortiz, and Randle W. Meisner. Latitudinal Variation of the Solar Photospheric Intensity. *The Astrophysical Journal*, 673:1209–1217, February 2008. ISSN 0004-637X. doi: 10.1086/524655.

Sabrina Sanchez, Alexandre Fournier, and Julien Aubert. THE PREDICTABILITY OF ADVECTION-DOMINATED FLUX-TRANSPORT SOLAR DYNAMO MODELS. *The Astrophysical Journal*, 781(1):8, December 2013. ISSN 0004-637X. doi: 10.1088/0004-637X/781/1/8.

J. M. da Silva Santos, K. Reardon, G. Cauzzi, T. Schad, V. Martínez Pillet, A. Tritschler, F. Wöger, R. Hofmann, J. Stauffer, and H. Uitenbroek. Magnetic Fields in Solar Plage Regions: Insights from High-sensitivity Spectropolarimetry. *The Astrophysical Journal Letters*, 954(2):L35, September 2023. ISSN 2041-8205. doi: 10.3847/2041-8213/acf21f.

Heinrich Schwabe. Sonnenbeobachtungen im Jahre 1843. Von Herrn Hofrath Schwabe in Dessau. *Astronomische Nachrichten*, 21:233, February 1844. ISSN 0004-6337. doi: 10.1002/asna.18440211505.

D. Sudar, I. Skokić, R. Brajša, and S. H. Saar. Steps towards a high precision solar rotation profile: Results from SDO/AIA coronal bright point data. *Astronomy & Astrophysics*, 575:A63, March 2015. ISSN 0004-6361, 1432-0746. doi: 10.1051/0004-6361/201424929.

K. F. Tapping. The 10.7 cm solar radio flux (F10.7). *Space Weather*, 11(7):394–406, 2013. ISSN 1542-7390. doi: 10.1002/swe.20064.

Appendix A. Download FITS Code

```python
"""
Script to download Fits file with the help of the sunpy package, from a
specific start date and a end date.  Also the interval length and
instrument  can be defined.
"""
import sunpy.net
from sunpy.net import Fido, attrs as a
from astropy import units as u

# Define the time range
start_time = '2023-12-04 20:00:00'
end_time = '2023-12-05 00:00:00'

# Define the search criteria
instrument = a.Instrument.hmi

data_type = a.Physobs.intensity
sample = 1 * u.hour  # Interval of the images, here every hour one image

# The search with the sunpy
results = Fido.search(a.Time(start_time, end_time), instrument,
                      data_type, a.Sample(sample))

# Download the data
downloaded_files = Fido.fetch(results)
print(f"Downloaded files: {downloaded_files}")
```

Listing A.1: The provided code outlines the commands used to download the required FITS files from the SDO/HMI instrument. This example demonstrates the download of 24 files from December 4, 2023, to December 5, 2023.

Appendix B. Sunspots Tacking Code

```python
import cv2
import numpy as np
from astropy.io import fits
from pathlib import Path
import matplotlib.pyplot as plt

def process_fit(fits_path:str):
    """
    Opens the fits image and normalize it that it can be used in the
    function to find the boxes around the spots(features)

    Args:
        fits_path (str): path to the fits file that should be used in
                         the func

    Returns:
        normalized_image (np.ndarry): normalized image between 0 and 255
    """

    # Open the FITS file and read the data
    with fits.open(fits_path) as hdul:
        data = hdul[1].data  # The 1 because in this fits files is the
                             # data is stored in the second position

    # Convert the image in to a ndarray
    image_data = np.array(data, dtype=np.float32)

    # Normalizing the image
    normalized_image =cv2.normalize(image_data, None, alpha=0,
                                    beta=255, norm_type=cv2.NORM_MINMAX,
                                    dtype=cv2.CV_8U)
    return normalized_image

def sun_infos(fits_path:str):
    """
    Extract all need information from the header of the FITS file and
    also calculate the sun_radius in pix.

    Assumptions:
    - Header of the data on second position
    - 'RSUN_OBS': observed radius of the sun in in arcsec
    - 'CDELT1': scale in arcsec per pix
    - 'CRPIX1','CRPIX1': x and y coordinate of the reference pix, here
                         the centerpoint of the solar disk
    - 'NAXIS2': resolution of the image assumed symmetrical
```

```

    Args:
        fits_path (str): path to the fits file

    Returns:
        sun_r_pix (int): sun radius in pix on the image
        sun_c (int): position of the sun center (x,y)
        res (int): resolution of the used image
    """

    with fits.open(fits_path) as hdul:
        header = hdul[1].header
        global sun_r
        sun_r = int(header['RSUN_OBS']/header['CDELT1'])
        sun_c = (int(header['CRPIX1']),int(header['CRPIX2']))
        res = int(header['NAXIS2'])

    return sun_c, res

def find_spots_and_boxes(image:np.ndarray, sun_radius:int,
                         sun_center:int, max_area:int=5000,
                         min_area:int=1000,max_distance_ratio:float=0.99,
                         min_distance_between_clusters:int=100):
    """
    Find the location of sunspots on the initial image. It uses the
    Connected Component Labeling method.

    Args:
        image (np.ndarray): The image where the spots should be found
                            image must be normalized between 0 and 255.
        sun_radius (int): Sun's radius on the image in pix
        sun_center (int): Pixel position of the solar disk center
        max_area (int, optional): Maximum area of the sunspots in pix.
                                  Defaults to 5000.
        min_area (int, optional): Minimal area of the sunspots in pix.
                                  Defaults to 1000.
        max_distance_ratio (float, optional): Maximum distance from the
                                              center. Defaults to 0.9.
        min_distance_between_clusters (int, optional): Minimum distance
                                                       between the spots.
                                                       Defaults to 100.

    Returns:
        grouped_boxes (tuple): (x_t,y_l,w,h) values for the boxes around
                                             the spots.
                               x_t,y_l top left corner of the box
                               w width of the box
                               h hight of the box
        grouped_centroid (tuple): (x,y) center point of the sunspots
    """

    # Preprocess the image
    image_blur = cv2.GaussianBlur(image, (13, 13), 0)
```

```
    binary_img = cv2.adaptiveThreshold(image_blur, 255,
                                       cv2.ADAPTIVE_THRESH_GAUSSIAN_C,
                                       cv2.THRESH_BINARY_INV, 301, 30)
    binary_img = cv2.dilate(binary_img, None, iterations=1)
    binary_img = cv2.erode(binary_img, None, iterations=1)

    # Find connected components
    _,_,stats, centroids = cv2.connectedComponentsWithStats(binary_img)

    # Filter spots based on area
    filtered_boxes = []
    filtered_centroid = []

    for label in range(1, len(stats)):
        area = stats[label, cv2.CC_STAT_AREA]
        #print(area)
        centroid = centroids[label]
        x, y, w, h = stats[label, cv2.CC_STAT_LEFT], stats[label,
                     cv2.CC_STAT_TOP], stats[label, cv2.CC_STAT_WIDTH],
                     stats[label, cv2.CC_STAT_HEIGHT]

        area_condition = (min_area < area) and (area < max_area)
        distance = np.linalg.norm(np.array(centroid) -
                                  np.array(sun_center))
        distance_condition = distance <= max_distance_ratio * sun_radius

        if area_condition and distance_condition:
            filtered_boxes.append((x, y, w, h))
            filtered_centroid.append(centroid)

    # Merge points too close to each other
    if filtered_centroid:
        grouped_boxes = []
        grouped_centroid = []

        for i in range(len(filtered_centroid)):
            current_centroid = filtered_centroid[i]
            current_box = filtered_boxes[i]

            # Check if the current point is close to any of the
            # existing groups
            merged = False
            for j in range(len(grouped_centroid)):
                group_centroid = grouped_centroid[j]
                group_box = grouped_boxes[j]

                # Use a distance threshold to decide if points are close
                distance_threshold = min_distance_between_clusters
                distance = np.linalg.norm(np.array(current_centroid) -
                                          np.array(group_centroid))

                if distance < distance_threshold:
                    # Merge the points manually by adjusting the
```

```
                    # bounding rectangle
                    x1 = min(current_box[0], group_box[0])
                    y1 = min(current_box[1], group_box[1])

                    x2 = max(current_box[0] + current_box[2],
                             group_box[0] + group_box[2])
                    y2 = max(current_box[1] + current_box[3],
                             group_box[1] + group_box[3])

                    new_group_box = (x1, y1, x2 - x1, y2 - y1)

                    new_group_centroid = 0.5 * (current_centroid +
                                                group_centroid)

                    grouped_centroid[j] = new_group_centroid
                    grouped_boxes[j] = new_group_box
                    merged = True
                    break

            # If the point didn't merge with any existing group, create
            # a new group
            if not merged:
                grouped_centroid.append(current_centroid)
                grouped_boxes.append(current_box)

        return grouped_boxes, grouped_centroid
    else:
        return [], []


if __name__ == "__main__":

    # Number of the TR series in the data/TR_0X folder
    TR = 1
    # Path of the folder
    file_path = np.genfromtxt('data/TR_0%i/names.txt'%TR,dtype=str)

    # Use the funtion to get keyfacts from the header
    sun_c, image_resolution = sun_infos(Path('data/TR_0%i'%TR)/
                                        file_path[0])

    # Generate a list of images from the fit files in the folder
    images = []
    for path in file_path:
        processed_fit = process_fit(Path('data/TR_0%i'%TR)/path)
        images.append(processed_fit)

    # Identify the initial position of the spots in the first image
    prev_image = images[0]
    bbox, centroid = find_spots_and_boxes(prev_image,sun_r,sun_c)

    prev_centroid = centroid

```

```
    print('Number of detected spots:',len(bbox))

    # Begin of the general tracking with the initial positions
    trackers = []
    lthickness = 3

    for idx, spot in enumerate(bbox):

        x1 = int(centroid[idx][0])
        y1 = int(centroid[idx][1])

        tracker = cv2.TrackerCSRT_create()  # Use CSRT tracker
        os  = 20 # oversize of the box (only for the better
                 # visualization)

        # Add the initial boxes as tracer
        tracker.init(prev_image,(spot[0]-os,spot[1]-os,spot[2]+os,
                                 spot[3]+os))
        trackers.append(tracker)

        for i in range(1, len(images)):
            current_image = images[i]
            current_image = cv2.cvtColor(current_image,
                                         cv2.COLOR_GRAY2RGB) #optional
            success, new_box = tracker.update(current_image)
            cv2.circle(current_image, (x1,y1), radius=2,
                       color=(150, 255, 0), thickness=-lthickness)

            if i == len(images)-1: #position in the last image
                                   #(necessary for the later calculation)
                x2 = new_box[0] + new_box[2] / 2
                y2 = new_box[1] + new_box[3] / 2
            if success:# Only zoom and continue if the tracking
                       # was successful, else skip to the next spot
                try:
                    # Zoom in to the currently tracing spot
                    zoom_oversize = 20
                    pos = 50
                    roi = current_image[new_box[1]-zoom_oversize:
                                        new_box[1]+new_box[3]+
                                        zoom_oversize, new_box[0]-
                                        zoom_oversize:new_box[0]+
                                        new_box[2]+zoom_oversize]
                    zoomed_roi = cv2.resize(roi,(0,0),fx=10,fy=10)
                    height, width, channels = zoomed_roi.shape
                    cv2.line(zoomed_roi,(int(width/2),0),
                             (int(width/2),height),(0, 0, 255),lthickness)
                    cv2.line(zoomed_roi,(0,int(height/2)),
                             (width,int(height/2)),(0, 0, 255),lthickness)
                    current_image[pos:height+pos,
                                  pos:width+pos] = zoomed_roi
                except:
                    continue
```

```
            else:
                continue

            # Draw bounding box on the current frame
            p1 = (int(new_box[0]-os), int(new_box[1]-os))
            p2 = (int(new_box[0] + new_box[2]+os),
                  int(new_box[1] + new_box[3]+os))
            cv2.rectangle(current_image, p1, p2, (0, 0, 255), 5)



            # Guidelines (all optional for easier visual follow)
            # Equator
            cv2.line(current_image,(0,sun_c[1]),
                     (image_resolution,sun_c[1]),(0, 0, 255),lthickness)
            # Initial x
            cv2.line(current_image,(x1,0),
                     (x1,image_resolution),(255, 0, 0),lthickness)
            # Initial y
            cv2.line(current_image,(0,y1),
                     (image_resolution,y1),(255, 0, 0),lthickness)
            # Moving x direction
            cv2.line(current_image,(int(new_box[0] + new_box[2] / 2),0),
                    (int(new_box[0] + new_box[2] / 2),image_resolution),
                    (0, 0, 255),lthickness)
            # Moving y direction
            cv2.line(current_image,(0,int(new_box[1]+new_box[3]/2)),
                     (image_resolution,int(new_box[1]+new_box[3]/2)),
                     (0, 0,255),lthickness)
            # Solar diameter
            cv2.circle(current_image,sun_c,sun_r,(255,0,0),lthickness)
            # Max distance from the solar center
            cv2.circle(current_image,sun_c,int(sun_r*0.9),(200,200,0),
                       lthickness)

            # Show the id of the spot in the upper left corner
            cv2.putText(current_image,"Spot ID: %i"%idx, (50, 80),
                        cv2.FONT_HERSHEY_SIMPLEX, 1, (0, 255, 0), 5,
                        cv2.LINE_AA)

            # Show the full modified image
            cv2.imshow('Traking Spot %i'%idx, current_image)
            # Wait for a key press (or use a delay to proceed automatic)
            cv2.waitKey(0)

        # Request if the spot should be included in the dataset or not
        append_condition = input('Want to include the trace? [y/n]')
        if append_condition == 'y':
            try:
                # Load existing data
                existing_data = np.genfromtxt(
                    "data/TR_0%i/data_points.csv"%TR, delimiter=',',
                    skip_header=True, dtype=float)
```

```
311             except IOError:
312                 # If the file doesn't exist, create a new array
313                 existing_data = np.array([]).reshape(0, 5)
314 
315             # Append the new values
316             new_row = np.array([x1, y1,x2,y2,(len(images)-1)])
317             updated_data = np.vstack([existing_data, new_row])
318 
319             # Save the updated data to the file
320             np.savetxt("data/TR_0%i/data_points.csv"%TR,updated_data,
321                   delimiter=',', comments="", fmt='%.8f',
322                   header="xcoor[pix],ycorr[pix],x2[pix],delta_time [h]")
323 
324     # Release the VideoCapture and close the window
325     cv2.destroyAllWindows()
```

Listing B.1: This listing outlines the code utilized for tracking sunspots on the solar surface. Specifically, line 185 assigns a track series number `TR`, in this instance '1', which stands for the tracking series 'TR_01', as detailed in the data structure outlined in Appendix D.

Appendix C. Calculation of the Rotation Rate Code

```python
import sunpy.map
import matplotlib.pyplot as plt
from astropy.coordinates import SkyCoord
import astropy.units as u
import numpy as np
from pathlib import Path
from scipy.optimize import curve_fit
from matplotlib.backends.backend_pdf import PdfPages

def fit_func(B_0,a,b):
    """
    Fit function in the common used form.

    Args:
        B_0 (float): Carrington heliographic latitude
        a (float): Equatorial rotation rate
        b (float): Factor that set the differential rotation

    Returns:
        float : Rotation for a specific latitude
    """
    return a + b * np.sin(np.deg2rad(B_0))**2

def cal_lon_and_lat(x_pix,y_pix,hmi_map):
    """
    Transformation from pix values to Carrington heliographic
    coordinates.

    Args:
        x_pix (float): X position of the spot in pix
        y_pix (float): Y position of the spot in pix
        hmi_map (sunpy.map): Sunpy hmi map from the used FITS file

    Returns:
        SkyCoord: The coordinates of the position on the solar surface
    """
    helioprojective_coords = hmi_map.pixel_to_world(x_pix * u.pix,
                                                    y_pix * u.pix)

    # Convert from helioprojective to heliographic coordinates
    heliographic_coords = helioprojective_coords.transform_to(
        SkyCoord(0*u.deg, 0*u.deg, 0*u.m, obstime=hmi_map.date,
                 observer = hmi_map.observer_coordinate,
```

```
                  frame='heliographic_carrington'))

    return heliographic_coords

def cal_omega_p(lon1,lon2,delta_t):
    """
    Calculation of the rotation rate and rotation period

    Args:
        lon1 (SkyCoord): Coordinate of the start position
        lon2 (SkyCoord): Coordinate of the end position
        delta_t (float): Time that separate the two measurements

    Returns:
        list: (omega,period) returns the rotation rate and period as a
              list
    """

    # Calculate longitudinal separation
    lon_sep = lon1.separation(lon2)

    # Convert time interval from hours to days
    delta_t_days = (delta_t / 24.0) *u.day

    # Calculate angular rotation rate (omega) in degrees per day
    omega = (lon_sep.deg / delta_t_days) * u.deg

    # Calculate period in days
    period = (360 * u.deg) / omega

    return omega, period

if __name__ == "__main__":

    # Numbers of the series that should be used for the calculation
    # and they must have the data_points.cvs in the directory
    tracking_series = [1,2,3,4]

    # Arrays that are used to stor the data
    lat_all = []
    omega_all = []

#-----------------------------------------------------------------------
    # Only plot configuration
    fig, ax = plt.subplots(figsize=(12, 8))
    ax.set_ylabel('Period [sidereal days]', fontsize = 20,)
    ax.set_xlabel('Latitude [deg]', fontsize = 20,)
    ax.set_title('Differential Rotation of Sunspots',fontsize = 25)
    ax.grid(True, ls = '--',linewidth = 0.8,)
    ax.tick_params(axis='both',labelsize=20)
#-----------------------------------------------------------------------

    with PdfPages('Plots_fits.pdf') as pdf:
```

```
        for trace in tracking_series:
            # Read in the datapoints
            file_path = np.genfromtxt('data/TR_0%i/names.txt'%trace,
                                      dtype=str)

            data_points = np.genfromtxt('data/TR_0%i/data_points.csv'
                                        %trace,delimiter=',',
                                        skip_header=True, dtype=float)

            # Generate the hmi maps from the start and end FITS
            # needed for the pix transformation
            hmi_map_start = sunpy.map.Map(Path('Data/TR_0%i'%trace)/
                                          file_path[0])
            hmi_map_end = sunpy.map.Map(Path('Data/TR_0%i'%trace)/
                                        file_path[-1])

            coor_1 = []
            coor_2 = []

            # Calculate the period
            for idx,row in enumerate(data_points):
                x1, y1, x2, y2,delta_time = row

                ax_s.plot(x1,y1, "o", color=col[idx],alpha = 0.7 ,
                          markeredgecolor='red', markeredgewidth=1,
                          markersize=10)
                ax_e.plot(x2,y2, "o", color=col[idx], alpha = 0.7,
                          markeredgecolor='red', markeredgewidth=1,
                          markersize=10)

                helio_cord1 = cal_lon_and_lat(x1,y1,hmi_map_start)
                helio_cord2 = cal_lon_and_lat(x2,y2,hmi_map_end)

                lat = np.mean([helio_cord1.lat.value,
                               helio_cord2.lat.value])

                omega, period = cal_omega_p(helio_cord1,helio_cord2,
                                            delta_time)

                lat_all.append(lat)
                omega_all.append(omega.value)

                ax.plot(np.abs(lat), period, "x",markersize = 8,
                          markeredgewidth=2,color= 'black')

# ------------------------------------------------------------------
            # Second plot configuration
            # Plot start and end image
            fig_pos = plt.figure(figsize=(20, 10))

            ax_s = plt.subplot(1, 2, 1, projection=hmi_map_start)
            ax_e = plt.subplot(1, 2, 2, projection=hmi_map_end)
```

```

            # Configure the plot
            ax_s.set_title("Start position\n%s"%hmi_map_start.date,
                           fontsize = 20)
            ax_e.set_title("End position \n%s"%hmi_map_end.date,
                           fontsize = 20)
            ax_s.set_xlabel("Projection  heliographic lon [arcsec]",
                            fontsize = 20)
            ax_s.set_ylabel("Projection heliographic lat [arcsec]",
                            fontsize = 20)
            ax_e.set_xlabel("Projection heliographic lon [arcsec]",
                            fontsize = 20)
            ax_e.set_ylabel("Projection heliographic lat [arcsec]",
                            fontsize = 20)
            fig_pos.suptitle("Tracemap %i"%trace,fontsize = 25)

            # Generate n random colors for better visualization
            col =[]
            for ii in range(0,len(data_points)):
                col.append((np.random.random(), np.random.random(),
                            np.random.random()))

            ax_s.imshow(hmi_map_start.data, cmap='gray', origin='lower')
            ax_s.invert_xaxis()
            ax_s.invert_yaxis()
            hmi_map_start.draw_grid(axes=ax_s, grid_spacing=15*u.deg,
                                    color="blue")


            # Plot the second map and draw its grid
            ax_e.imshow(hmi_map_end.data, cmap='gray', origin='lower')
            ax_e.invert_xaxis()
            ax_e.invert_yaxis()
            hmi_map_end.draw_grid(axes=ax_e, grid_spacing=15*u.deg,
                                  color="red")

            # Save plot
            pdf.savefig(fig_pos)
#-------------------------------------------------------------------

        lat_all = np.array(np.abs(lat_all))
        omega_all = np.array(omega_all)

        # Save plot  with out fit function
        pdf.savefig(fig)

        # Fit in the plot, and calculate the R^2 value
        popt, pcov = curve_fit(fit_func, lat_all, omega_all)
        uncertainties = np.sqrt(np.diagonal(pcov))
        residuals = omega_all - fit_func(lat_all, *popt)
        ss_res = np.sum(residuals**2)
        ss_tot = np.sum((omega_all -np.mean(omega_all))**2)
        r_squared = 1 - (ss_res / ss_tot)
```

```
203
204         # Print the R^2 and fit values
205         print(r_squared)
206         print(popt)
207
208         # Latitudes to plot the fit function
209         lat1 = np.arange(np.min(lat_all),np.max(lat_all),1)
210
211         # Plot the fit function
212         ax.plot(lat1,360/fit_func(lat1,*popt),color = "green")
213
214         # Annotate fitted values in the plot
215         ax.annotate("$\\Omega(B) = %.3f %.3f \cdot \sin^2(B)$"
216                 %(popt[0],popt[1]), xy=(16,26.5),
217                 xytext=(0.04,4/5), textcoords='axes fraction',
218                 bbox = dict(facecolor='grey', alpha=0.5,
219                             edgecolor='None', pad=10.0),fontsize=15,
220                             arrowprops=dict(facecolor='green',
221                                             shrink=0.02, width=0.25,
222                                             headwidth=5, headlength=7))
223
224         plt.tight_layout()
225
226         # Show the plot
227         plt.show()
228
229         # Save plot with the fit function
230         pdf.savefig(fig)
```

Listing C.1: The code illustrates the necessary calculations for determining the rotation rate using data points obtained from the sunspot tracking process. The *data_points.csv* file must be located in the correct directory, as indicated in Appendix D. The `tracking_series` array, in line 80, reveals that four tracking series are used in the calculation.

Appendix D. Directory Structure

```
Solar Rotation Code
├── data
│   ├── TR_01
│   │   ├── data_points.csv ..... File generated by Sunpots_tracking.py
│   │   ├── Image_01.fits
│   │   ├── Image_02.fits
│   │   ├── ⋮
│   │   └── names.txt ... Terminal command 'ls >> names.txt' in the dir to generate
│   ├── TR_02
│   │   ├── data_points.csv
│   │   ├── Image_01.fits
│   │   ├── Image_02.fits
│   │   ├── ⋮
│   │   └── names.txt
│   └── ⋮
├── Download_fits.py ..... Appendix A
├── Sunpots_tracking.py ..... Appendix B
├── Calculation.py ..... Appendix C
└── Plots_fits.pdf ... Automatically saved plots after execution of Calculation.py
```

Figure D.1.: This figure shows the directory and data structure necessary to ensure the codes functionality. The *names.txt* file lists the names of all FITS files in the directory that should be used for the tracking. Files highlighted in gray are generated by the code itself.